Impact of Wind Generation on Line Protection

Alberto Castañon[1], Roberto Cimadevilla[1], Pablo Eguia[2], Esther Torres[2], Ricardo Ibarra[2]

[1]ZIV Automation, Parque Científico y Tecnológico de Bizkaia, 210. 48170 Zamudio, Bizkaia, Spain T: +34 94 452 20 03, www.ziv.es

[2]Universidad del País Vasco / Euskal Herriko Unibertsitatea, Barrio Sarriena s/n 48940 Leioa, Bizkaia.

*Contact Author: Parque Tecnológico, 210 48170 Zamudio (Vizcaya) - España Tel: +34 600570508 – Email: alberto.castanon@zivautomation.com

ABSTRACT:

Renewable energy-based generation like photovoltaic or wind farms present a different response to short circuit than conventional synchronous generators due to their coupling trough power electronics-based inverters. Those inverter-based resources behave like current sources as opposed to voltage sources and their short circuit current, including negative sequence component, is highly determined by their control system. Therefore, protection functions like directional and non-directional overcurrent, phase selector, distance protection and directional comparison might malfunction. This paper introduces the basic concepts of Wind Turbines (WT) and their fault response, analyzing their impact on the aforementioned function protections.

Keywords: protection relays; fault identification; renewable energy; wind turbine; photovoltaic generator; incremental quantities, directional, distance

_____

1. INTRODUCTION

Fault response of a synchronous generator is well known, and current protection functions are designed to work accordingly. For example, in the case of an asymmetrical fault, a negative sequence voltage arises at the generator terminals, for which, given the small and mainly reactive impedance that the generator represents a 90⁰ lagging negative sequence current (I2) is developed. Same behavior is found for positive sequence current (I1). This behavior allows protection functions to correctly identify a fault, its direction, fault type and involved phases. However, WT response might be different, and therefore, protection engineers and manufacturers are in need to review the impact that a grid with increased introduction on wind energy will have on the performance of their protection algorithms. In [1] the lack of a normally present I2 is identified as the main driver for malfunction of protection units. However, current IBR technologies allow for I2 injection, being the angle related to V2 with which this current is injected the main concern, just as the angle of I1.

Despite of IBRs current contribution being heavily dependent on control strategy used [2], standard models of WTs does not take in account control strategy, and if so, they only represent active and reactive power grid code compliance for symmetrical voltage dips like in [3], [4], [5] or asymmetrical dips but complying to older grid codes like [6] in which no treatment is given to negative sequence components and often no mention of type of control used is done. In this work, the control of a Type III and IV is modelled using MATLAB Simulink®, taking in account latest grid code requirements, so different protection functions can be tested.

2. WIND TURBINE TYPES

Independently of the primary source of energy, the impact of renewable energy on the electrical system is determined by the type of interface the generator has with the grid. First type of wind turbines were induction generators, considered "fixed speed" types since their synchronous speed is given by the machine number of poles and the grid frequency, which makes them inflexible and

caused them to be replaced by the Type II [7], in which the speed can be controlled by interfering the rotor circuit with variable resistance. Given the inefficiency this method represents, they have been currently replaced by the Type III and IV, which use power electronic based inverters and in which this study is focused. A further division of the Type IV classification is made in [8] since recent developments already available on the market include full converter machines equipped with gearbox but this work will take all full converter equipped machines as one single Type IV category.

2.1   TYPE III

Type III WTs are the evolution of Type II and II WTs, but in this case a double feed induction generator (DFIG) is used. On a DFIG, the stator is directly connected to the grid and the rotor is connected with a back to back power electronic based converter, with rating of around 25%-30% of the turbine rated power, which allows to modify operation speed. The power converter is comprised of Rotor Side Conveter (RSC), Grid Side Converter (GSC) and a coupling capacitor which acts as a buffer. RSC allows to control the flow of active power by controlling the current in phase with the stator voltage and the reactive power by controlling the current in quadrature.
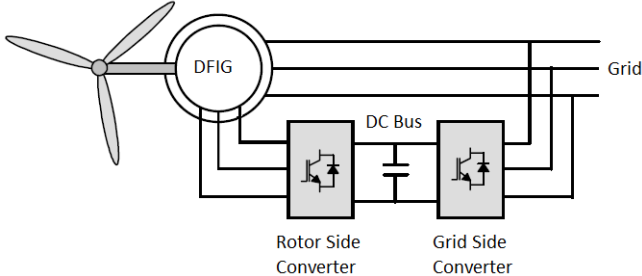
Fig. 1 Type III Wind Turbine [7]

2.2   TYPE IV

The full-scale WTS mainly consists of a variable speed-controlled generator, connected to the grid through a full-scale back-to-back power converter, rated to 100% of the turbine output power as it is shown in Fig. 2. The generator can be an asynchronous generator (AG), an electrically excited synchronous generator (EESG) or a Permanent Magnet Synchronous Generator (PMSG). In addition, the gearbox is not necessary in this case since the usually used generators can operate at lower speeds due to their high number of poles [8].
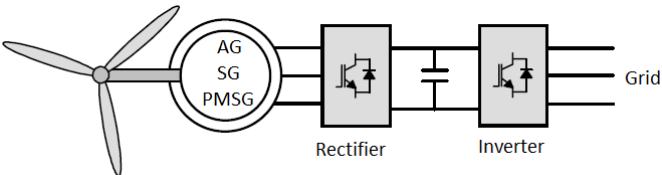
Fig. 2 Type IV Wind Turbine [7]

During normal operation, the control system of the converters is structured in an external and internal loop. Based on active and reactive power settings, external loop creates current references, which the internal control loop takes as input to provide the converter with the voltage reference to be placed at converter terminals.

3.   FAULT RESPONSE OF WIND TURBINES

3.1   TYPE III

On a DFIG, stator terminals are directly connected to the grid. As a result, the initial transient response following a sudden voltage drop (as a result of grid fault) is dominated by the demagnetization of the induction machine which may result in high stator peak currents [12]. This stator overcurrent is transmitted, due to the magnetic coupling, and the laws of flux conservation [7], to the rotor windings [13]. These overcurrent's, which can be up to three times the nominal value of the current, can damage the rotor and stator windings, but can be especially critical for the semiconductors of the RSC, that can reach thermal breakdown [14]. A good vectorial explanation of this phenomena is given in [15].

To be able to understand the impact that a fault on the line has on the rotor it is important to notice that the voltage on the rotor depends on the current circulating through it, and also the voltage induced by the stator $\vec{v}_o^r$ as shown in the following equation:

$$\vec{v}_r^r = \vec{v}_o^r + R_r' \cdot \vec{\imath}_r^r + L_r' \frac{d}{dt} \vec{\imath}_r^r$$

Where $\vec{v}_r^r$ is rotor voltage, referred to the rotor, $\vec{\imath}_r^r$ is rotor current, referred to the rotor, R_r' and L_r' are the machine resistance and inductance. $\vec{v}_o^r$ is produced by three different voltage components, called direct $\vec{v}_d^r$, inverse $\vec{v}_i^r$ and free $\vec{v}_f^r$.

$$\vec{v}_o^r = \vec{v}_d^r + \vec{v}_i^r + \vec{v}_f^r$$

On steady state, stator voltage creates a rotating magnetic flux, which is proportional to the magnitude of such voltage called direct flux, which creates $\vec{v}_d^r$ on the rotor. Since, referred to the stator voltage, the rotor is moving at slip frequency, $\vec{v}_d^r$ magnitude is proportional to the slip and its frequency is that of the slip. If a fault occurs, this voltage drops down quickly, but since flux cannot change instantaneously, a transient stator flux component is developed, which is fixed as seen by the stator and decays with time. This component is called free flux and creates a voltage component on the rotor $\vec{v}_f^r$ which is proportional to the voltage drop caused by the fault, and, from the rotor perspective, it rotates at the stator electrical speed. If the fault is unbalanced, the negative sequence component of the stator voltage creates a flux, which rotates on inverse direction, creates the third component of the rotor voltage $\vec{v}_i^r$, which seen by the rotor, rotates at double the synchronous speed.

Furthermore, the surge following the fault includes a "rush" of power from the rotor terminals towards the converter. As the grid voltage drops in the fault moment, SGC is not able to transfer the power from the RSC to the grid and therefore the additional energy goes into charging the DC bus capacitor [16], dangerously rising its voltage. In order to protect RSC the most extended solution is based on the use of a protective circuit known as crowbar. This device consists of a three-phase diode bridge for AC/DC conversion, and a switching device such as a GTO in series with a small resistance on the DC side. When an over-current condition is detected, the GTO is switched from the off to the on state and shorts the rotor windings, therefore bypassing and protecting the RSC [9] but also blocking Q and P control, leaving the DFIG working as a common induction machine. In case of unbalanced faults, since the inverse flux does not decay, crowbar activation can last for the entire fault duration. Two main solutions used to avoid crowbar activation and its subsequent control lost are demagnetizing control and DC Chopper. First solution consists of bypassing steady state control of the RSC during under voltage events to orientate RSC current injection towards reducing transient rotor currents and minimize occurrence of crowbar interruptions. Second solution consists of the addition of a DC Chopper connected on the DC Bus. This Chopper consists of a set of resistances installed in parallel to the DC converter capacitor, which in case of severe grid fault will limit over voltages in DC link, while resistances dissipate the energy that cannot be delivered to the grid due to the short circuit.

A third solution to avoid lose of control during crowbar activation has been lately implemented. It consists of an active crowbar circuit, which is similar to the usual (passive) crowbar but interfered with IGBT switches instead of GTOs and therefore controllable, which bypasses the fault currents from RSC while still providing limited control during grid fault conditions. Providing reactive power support through the GSC to partially offset the Q consumed by the WT. This modern scheme is left outside of this scope of this study.

3.2 TYPE IV

Type IV WTs are fully coupled to the grid through their power converter; therefore, their fault response is totally determined by the control strategy implemented to comply with Low Voltage Ride Trough (LVRT) requirements by grid codes. When a fault occurs, LVRT mode takes over the external loop to provide the internal loop with the current references the grid codes demand to be injected. In case of an asymmetrical fault, a negative sequence component of voltage (V2) is developed, and therefore, the control system must take into account both direct (I1) and inverse (I2) components of current. First approaches to inverse components were to suppress the injection of I2. However, the absence of I2, in presence of V2 might cause double frequency oscillations, besides the clear disadvantage for protection systems of not counting with I2. Nowadays, grid codes have evolved to adapt to a higher penetration of renewable energy, as highlighted in [23], system operators demand I2 injection in case of asymmetrical faults, with the main purpose of reducing power oscillations, reducing DC voltage on the coupling capacitor [24], besides reducing negative sequence voltage, which brings a reduction of overvoltage at healthy phases [25]. Recent European grid codes like the VDE-AR-N 4120 in Germany, or the P.O. 12.2 in Spain, take I2 injection requirement further by specifically requiring reactive I2 current, which makes a Type IV short circuit response closer to that of a conventional synchronous generator, which represents a totally reactive impedance in both positive and negative sequence, or in other words, impedances with a 90⁰ angle. Therefore, as written in [26], [24], [27] and [25] a model of a WT that represents a double sequence control is essential for short circuit studies.

Modern grid codes require I1 and I2 to be injected proportionally to the change in their respective voltage components by a k factor as shown in Fig. 3.
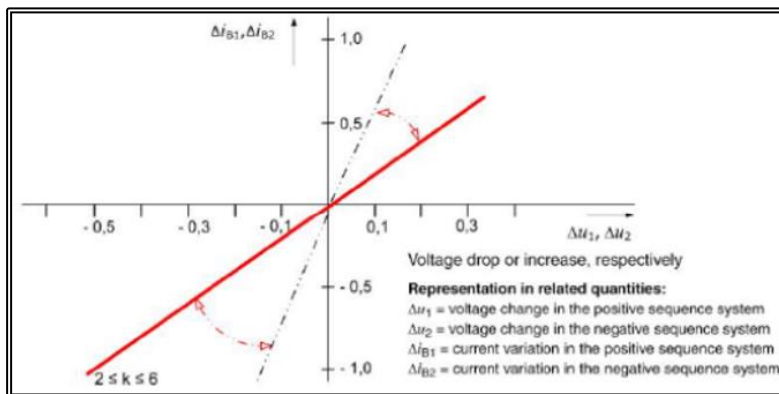
Fig. 3 Proportional injection of current for LVRT mode according to VDE-AR-N 4120

Current to be injected cannot exceed physical limits of the converter, and therefore current components need to be prioritized and limited accordingly. The main purpose of the LVRT mode is to support voltage level by injecting reactive current and the secondary is to contribute to stability by injecting active power; priority is usually given to reactive components. As stated in [28], the value of K factor, as much as the limiting of each reactive and active component on both sequences has an influence on the angle of the current injected and therefore on the impedance that the WT represents to the grid. This might cause the protection functions that rely on the value of those impedances to fail.

4. IMPACT ON PROTECTION FUNCTIONS

Due to the differences found between the fault response of a synchronous generator and both types of wind turbines, following protection functions were tested.

4.1 DIRECTIONAL OVERCURRENT

This function takes advantage of the phase change between voltage and current since the polarity of a current changes for a forward or reverse fault. Different sequence magnitudes can be used to detect this direction. For a forward fault, the current is expected to lag the voltage at a maximum of the line impedance, while, for a reverse fault, the phase difference between voltage and current is expected to be closer to 180º. In this work, positive sequence directional (67P), pure-fault positive sequence directional (67ΔP), negative sequence (67Q) and phase current polarized with positive-sequence voltage memory (57P21) usually used for distance are studied.

4.2 PHASE SELECTOR

Angular relationship between voltage components present during a fault are given by the sequence network that represents the fault. Since the impedances that normally compose the electrical system are mainly inductive, these angular relationships are expected to be translated to sequence currents, which are normally available in sufficient quantity to declare faulted phase. However, in presence of wind energy, the impedance represented by the source is modified by the control system and current angular relationships might not be trustworthy. Furthermore, algorithms that compare I0 and I2 (φ_{I0}), might fail in absence of I2 or if the angle at which it is injected is changed by the control system.

Phase selector algorithms that compare the angle between I2 and I1 (φ_{I1}) or ΔI1 might fail due to the difference between the homogeneity of the fault and pre-fault sequence networks. Superposition principle, usually used to decomposed current in fault and pre-fault components can still be applied for inverter bases resources if we replaced a current source by a voltage source with a series impedance. Nevertheless, I1 limitation by the control system generate positive sequence pure fault impedance angles higher than 90º, increasing the non-homogeneity of the pure fault positive sequence circuit. This makes the angle between ΔI1 and I2 to differ from the expected.

As a solution to this problem, in this work a phase selector algorithm based on voltage sequence angular relationship is proposed, which are deducted from the sequence network for different faults. In Fig. 4, the sequence networks connection for an AG fault is shown, where Z1SL, Z2SL and Z0SL represent local positive, negative and zero sequence impedances. Z1SR, Z2SR and Z0SE represent remote source impedances. Z1LF, Z2LF Y Z0LF represent line impedances up to the fault location and Z1LF`, Z2LF` Y Z0LF` line impedances on the remote side of the line. E1SL and E1SR represent local and remote voltage sources and RG ground fault resistance.
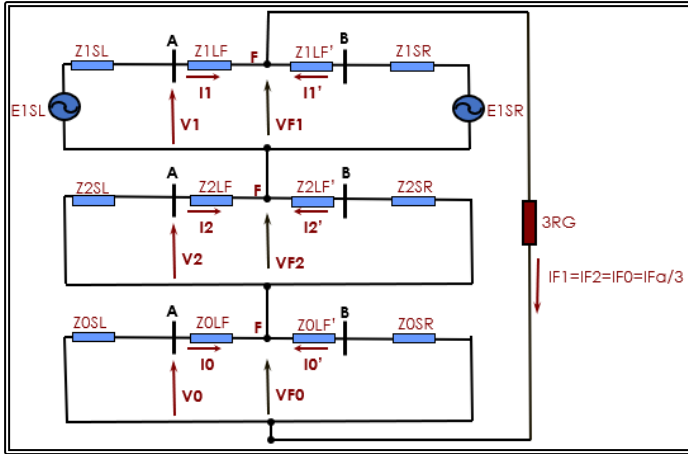
Fig. 4 Sequence networks connection for an AG fault.

Since for a single-phase fault IF1=IF2=IF0, the ratio between negative and zero sequence voltages at fault location is:

$$\frac{VF2}{VF0} = \frac{Z2par}{Z0par} \tag{1}$$

Where Z2par and Z0par are the equivalent impedance of the negative and zero sequence networks. Voltage relationship seen by the relay can be expressed as:

$$\frac{V2}{V0} = \frac{VF2}{VF0} * \frac{Z2L * Z0SL}{Z0L * Z2SL} = \frac{Z2par}{Z0par} * \frac{Z2L * Z0SL}{Z0L * Z2SL}$$

And, since the impedance angles of the negative and zero sequences are generally similar, taking the sequence components based on phase A, the angle between V2 and V0 (φ_{V0}) for an AG fault will be 0º. For an ABC system, the angle for a BG fault will be -120º and 120º for a CG fault.

To find the angular relationship at fault location for VF2 and VF1 we can use the fact that VF1+VF2+VF0=IF1*3RG, plus VF1=IF1*Z2par and VF2=IF1*Z2par.

$$\frac{VF2}{VF1} = -\frac{Z2par}{3RG + Z2par + Z0par} \tag{2}$$

Therefore, for an AG fault, the angle between VF2 and VF1 ($\varphi1$) would be 180º. Considering an ABC system, again, 60º for a CG fault and -60º for a BG fault. No much phase shift is expected between the quantities at the fault location and the ones at the relay location, since the current coming from the WT is limited. It is important to mention that in this case, the use of pure fault positive sequence voltage $\Delta V1$, does not improve the algorithm performance, since, given the angular difference between Z1SL and Z1LF, $\Delta V1$ could have a high angle difference with respect to VF1.

According to (2), the phase difference between VF1 and VF2 increases with higher fault resistance, nevertheless, with fault resistance, the angle difference between VF1 and V1 decreases because the magnitude of I1 is smaller.

For a two-phase fault to earth, the sequence networks connection is shown in Fig. 5.
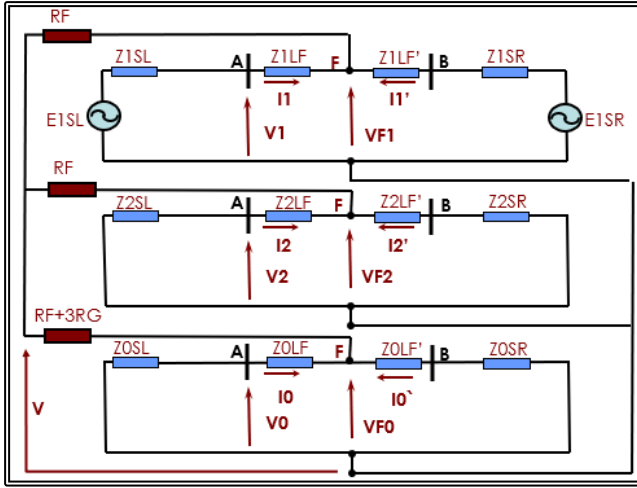
Fig. 5 Sequence networks connection for a two-phase to ground fault.

Where RF stands for fault resistance between phases. Out of Fig. 5, it can be inferred that the voltage between the fault location and ground can be calculated using again the parallel equivalent of the sequence impedances: Z2par and Z0par.

$$V = IF1 * \frac{(RF + Z2par) * (RF + 3RG + Z0par)}{(RF + Z2par) + (RF + 3RG + Z0par)}$$

$$IF2 = -\frac{V}{RF + Z2par} = -IF1 * \frac{(RF + Z2par) * (RF + 3RG + Z0par)}{(RF + Z2par) * (RF + Z2par) + (RF + 3RG + Z0par)}$$

$$\frac{IF2}{IF1} = -\frac{RF + 3RG + Z0par}{2RF + 3RG + Z0par + Z2par}$$

Considering that, for the positive and negative sequence networks:

VF2=-IF2*Z2$_{par}$

VF1=E1-IF1* Z1$_{par}$

And using the voltage loop shown as V and positive sequence.

$$E1 - IF1 * Z1par - IF1 * RF = IF1 * \frac{(RF + Z2par) * (RF + 3RG + Z0par)}{(RF + Z2par) + (RF + 3RG + Z0par)}$$

$$E1 = IF1(Z1par + RF + \frac{(RF + Z2par) * (RF + 3RG + Z0par)}{(RF + Z2par) + (RF + 3RG + Z0par)})$$

$$VF1 = IF1(RF + \frac{(RF + Z2par) * (RF + 3RG + Z0par)}{(RF + Z2par) + (RF + 3RG + Z0par)})$$

$$\frac{VF2}{VF1} = \frac{(RF + 3RG + Z0par) * Z2par}{(2RF + 3RG + Z0par + Z2par)(RF + \frac{(RF + Z2par) * (RF + 3RG + Z0par)}{(RF + Z2par) + (RF + 3RG + Z0par)})} \tag{3}$$

In which, taking for now RF and RG as zero, and using sequence components referred to phase A, the angle between VF2 and VF1 ($\varphi V1$), is 0° for a BCG, 120° for a CAG and -120° for a ABG fault.

Taking into account the voltage loop between negative and zero sequence:

$$IF2 * (Z2par + RF) = IF0 * (Z0par + RF + 3RG)$$

$$\frac{IF2}{IF0} = \frac{Z0par + RF + 3RG}{Z2par + RF}$$

And that for the zero-sequence network: $VF0 = -IF0 * Z0_{par}$

The relationship between sequence voltages is:

$$\frac{VF2}{VF0} = \frac{Z0par + RF + 3RG}{Z2par + RF} * \frac{Z2par}{Z20par} \tag{4}$$

Which, ignoring for now RF and RG the angle between VF2 and VF0 (φ_{V0}) is again 0° for a BCG fault. 120° for a CAG and -120° for a ABG. It should be noted that, even in absence of I2 injection, Z2par is still valid since it would at least be considering Z2SR.

By inspecting formulas (1), (2), (3) and (4), it is notorious that there are 4 fault conditions that could deviate the actual angular relationship from the theoretical value found. RF, RG, angular difference between impedances of a determined sequence network, or non-homogeneity (NH), whether it is negative (NH_2), zero (NH_0) or non-homogeneity among them (NH_{20}). Since RF does not usually reach high values, it is excluded from the analysis. To find the limits to which φ_{V1} and φ_{V0} can be displaced by these factors, mathematical relationships found where simulated with different values of RG, NH_2, NH_0 y NH_{20}, for a maximum RG of 200 Ohm and maximum non-homogeneity of 20°.

Table 1 Limit deviation of angular relationships.

	Single Phase Fault		Phase to Phase to Ground Fault	
	φ_{V0}	φ_{V1}	φ_{V0}	φ_{V1}
RG	No impact	$+80^\circ$	-80°	No impact
NH_2	$\pm3.3^\circ$	$\pm3^\circ$	No impact	No impact
NH_0	$\pm3.3^\circ$	$\pm3^\circ$	No impact	No impact
NH_{20}	$\pm20^\circ$	$\pm16^\circ$	No impact	No impact

From Table 1 it can be seen that grid non-homogeneity has a tolerable impact on voltage angular relationships, but taking in account the displacement due to RG for φ_{V1} on phase to ground faults and φ_{V0} for phase to phase to ground faults it is convenient to rotate the found angles to define the following areas for faulted phase selection.
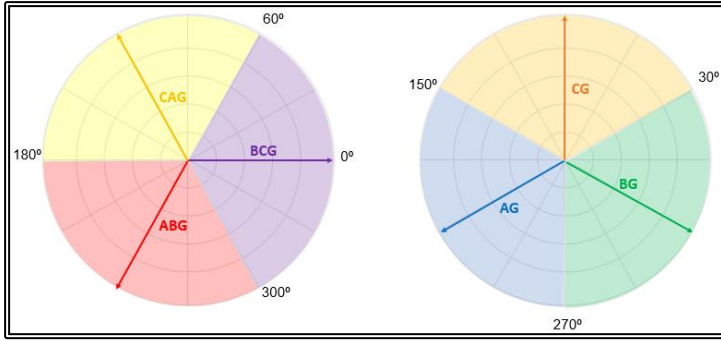
Fig. 6 φV1 Angular zones for faulted phase selector.
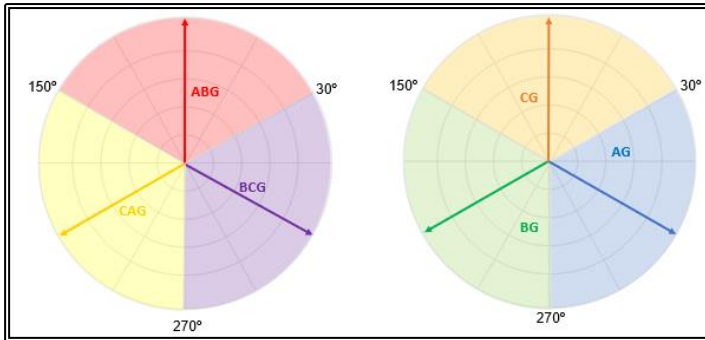
Fig. 7 φV0 Angular relationships for faulted phase selection.

By using levels of V2 and V0 it is possible to detect asymmetrical or ground faults, selecting the precise phase using measured φV1 and φV0. φV1; zones found for ABG, BCG and CAG faults are also valid for AB, BC and CG faults.

A second option to differentiate between phase to phase to ground and single phase to ground faults is using impedance zones. For example, for an AG fault, distance AG zone will be asserted but no BCG zone will, while for a BCG fault no AG zone would be asserted.

4.3   DISTANCE PROTECTION

4.3.1   Fault Resistance Impact on Distance Protection

The impact that fault resistance has on distance protection is explained on [32]. The equations that represent voltage drop for an AG of BC(G) fault are:

$$Va = Ieq \cdot Z1LF + IFa \cdot RF, \text{ where } Ieq = Ia + I0 \cdot \left(\frac{Z0L}{Z1L} - 1\right)$$

$$Vbc = Ibc \cdot Z1LF + IFbc \cdot RF/2, \text{ where } IFbc = IFb - IFc$$

In general, for any type of fault, the following expression can be used: $Vr = Ir \cdot Z1LF + IF \cdot RF \cdot k$, where Vr and Ir are local voltage and current used for each fault type, If is current that circulates through the fault resistance and K a constant (k=1 for single phase faults and K=1/2 for multi-phase faults. Dividing all factors by Ir, impedance seen by distance units is $Zr = Z1LF + \frac{IF}{Ir} \cdot RF \cdot k$. As seen in Fig. 8, the impedance see by the relay is not the positive sequence impedance up to the fault location, but a new factor is added, $\frac{IF}{Ir} \cdot RF \cdot k$, called apparent fault resistance.
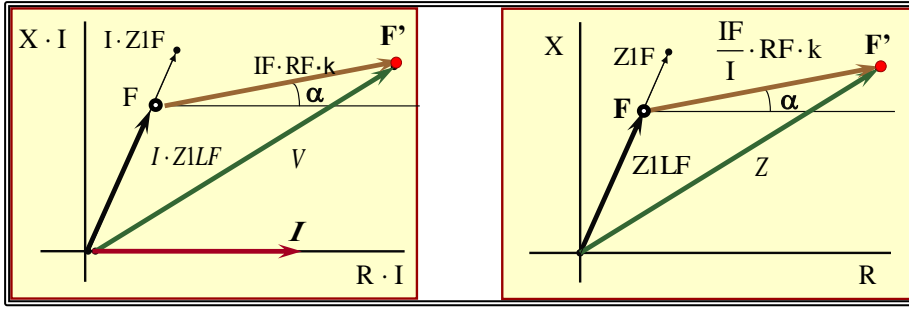
Fig. 8 Impedance seen by relays on a) voltage diagrams (R*I -X*I), and b) impedance diagrams (R-X).

Whenever there is current flowing from the remote side IF will be higher than Ir and apparent fault resistance will be higher than real fault resistance. This amplifying effect of fault resistance is higher when the difference between local and remote current is higher. Wind generators can be considered as weak sources, with a low positive and negative sequence current contribution with regard to the network fault current contribution. Nevertheless, it has to be noted that, for ground faults (faults with normally higher fault resistance), the power transformer at the output of the windfarm, usually delta (MV voltage winding, windfarm side) / star grounded (HV winding, network side), provides a high zero-sequence current. This makes the windfarm fault current contribution to be in the same order as the network one, so the amplification of the apparent fault resistance is low. This amplification will be high for ungrounded faults but normally this kind of faults do not normally have a high fault resistance.

Apparent fault resistance shows α angle due to the phase difference between Ir and IF, which mainly depends on two factors, load and system non-homogeneity.

4.3.2 Compensation of Apparent Fault Resistance

Load compensation is described on [32]. Different polarization methods for the reactance line are given depending on the fault type. For a single-phase to ground fault, polarization can be achieved by I2, I0, $Iph\text{-}Iph_{prefault}$, $I1\text{-}I1_{prefault}$, etc. For a two-phase fault, to ground or not, $Iphph\text{-}phpb_{prefault}$ or I1-I1prefault can be used. Work on [32] also explains the influence of the sequence network non-homogeneities in the apparent fault resistance angle. Inverter bases resources like WTs represent different issues for this compensation:

Positive sequence network: Since the method used to compensate the load uses $I1\text{-}I1_{prefault}$ as polarization phasor, the homogeneity of the pure fault network has an impact on it. Inverted based resources might work as current sources under fault condition. As it was mentioned in point 3.2, the fault current limitation produced by the IBR makes the positive-sequence pure fault source impedance reach angles higher than 90º. This creates a high non homogeneity of the pure fault positive-sequence network. Besides, the fault current limitation makes the magnitude of mentioned impedance be high and so its weight on the non homogeneity level is important.

Negative sequence network: As previously stated, WTs might not supply I2 or inject it at a different angle than 90º referred to V2.

In [32] and [33], a non-homogeneity compensation of the system is done based on the impedance values of the local source, remote source, line, and parallel equivalent circuit. Since the most used polarization methods are through I2 and Iphph-Iphph_prefault, non-homogeneity compensation is done through the following formula.

$$\frac{Ir}{IF} = \frac{Z1SR}{Z1SL + Z1L + Z1SR} \tag{5}$$

In (5) a high value for the equivalent parallel circuit impedance and a fault at 100% of the line are considered; this last assumption creates a small tolerable error. Z1L and Z1SR are adjustable through setting values. However, the value of Z1SL depends on the control system of the WT and therefore

need to be measured and corrected for in real time. Since load compensation uses the positive pure fault network, pure fault Z1SL must be measured, for which the following formula is proposed:

$$Z1SL = \frac{-(V1 - V1prefault)}{(I1 - I1prefault)}$$

Once Z1SL is measured, the following methods to compensate the apparent fault resistance in presence of wind generation are described.

4.3.2.1　Compensation of Apparent Fault Resistance- Single Phase Faults
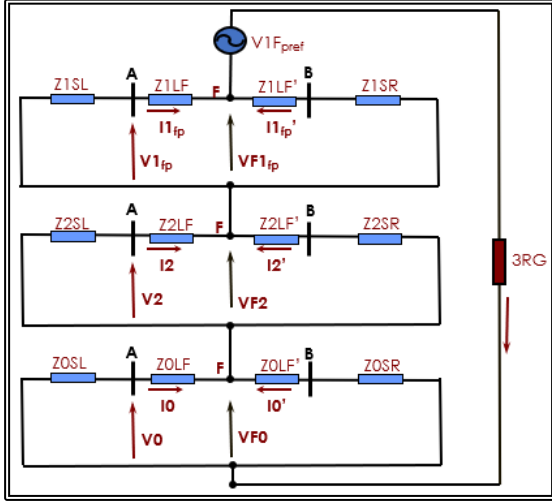
Fig. 9 Pure-fault sequence networks connection for an AG fault.

If the WT provides I2, like in the case of the Type III or Type IV, if compliance for the latest grid codes are implemented, I2 can be a valid polarization phasor. Non-homogeneity compensation if I2 is used must be accounted for with the following formula, $I2 * \frac{Z2SL+Z1L+Z1SR}{Z1SR}$., in which the following assumptions are made: Z2L=Z1L and Z2SR=Z2SR and Z2SL can be calculated by $Z2SL = \frac{-V2}{I2}$. Nevertheless, negative sequence network is normally fairly homogeneous.

If no I2 is injected by the WT, I0 can also be used as a polarization phasor. Non-homogeneity compensation for the zero-sequence network could be done by the following formula $I0 * \frac{Z0SL+Z0L+Z0SR}{Z0SR}$. Z0SL could be calculated by $Z0SL = \frac{-V0}{I0}$. Nevertheless, zero sequence network is normally fairly homogeneous.

Iph-Iph$_{prefault}$ is not recommended as a polarization phasor since it is affected by the non-homogeneity of the pure fault positive sequence network, which might be very high. Anyway, this homogeneity could be compensated with the formulas shown before.

4.3.2.2　Compensation of Apparent Fault Resistance- Phase to Phase Faults

If I2 is provided by the WT, it could be used as a polarization phasor.

On a BC fault the following relations are valid.

$$Vb - Vc = (Ib - Ic) * Z1LF + (IFb - IFc) * RF \tag{6}$$
$$IFb - IFc = (I1Fa - I2Fa) * (-j * \sqrt{3}) \tag{7}$$

Since IF1=IF2, then, (I1F-I2F)=-2*I2F　and therefore I2 can be used. To compensate non-homogeneity, $I2 * \frac{Z2SL+Z1L+Z1SR}{Z1SR}$ could be used. If the WT does not inject I2, $(I1 - I1prefault) * \frac{Z1SL+Z1L+Z1SR}{Z1SR}$ could be used as a polarization phasor.
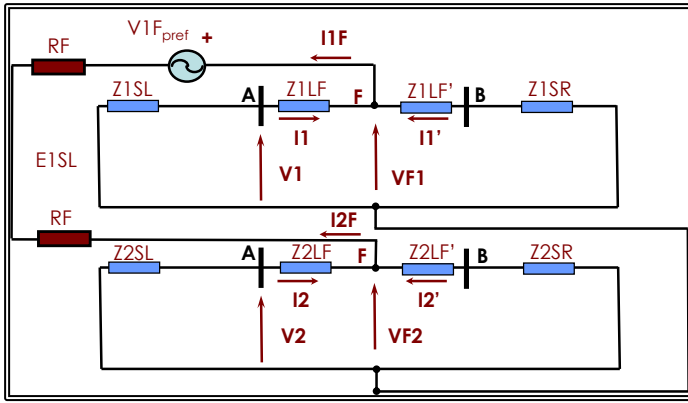
Fig. 10 Pure fault sequence networks connections for a phase to phase fault.

4.3.2.3 Compensation of Apparent Fault Resistance- Phase to Phase Ground Faults

On a phase to phase to ground fault, equations (6) and (7) are satisfied. Taking into account the circuit in Fig. 11, the following expression can be deducted as a valid polarization phasor.

$$I1F - I2F = \frac{Z1SL + Z1L + Z1SR}{Z1SR} * \left(I1 - I1_{prefault}\right) - \frac{Z2SL + Z1L + Z1SR}{Z1SR} * I2$$
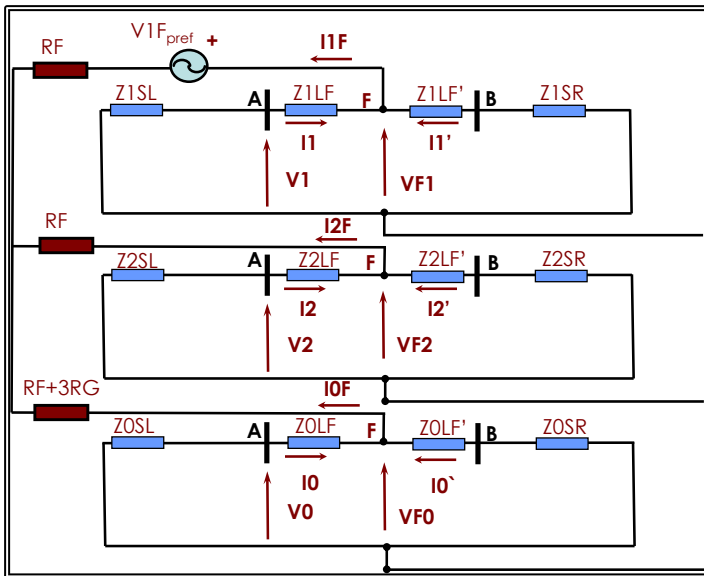
Fig. 11 Pure fault sequence network connections for a BCG fault.

4.3.2.4 Compensation of Apparent Fault Resistance- Three Phase Faults

Following the same method, a valid polarization phasor for three phase faults would be:

$$\frac{Z1SL + Z1L + Z1SR}{Z1SR} * \left(I1 - I1_{prefault}\right).$$

4.3.3 Directional Comparison Units

On [30] and [33], units comparing the angle of the current from both ends on the line are described, which improve line differential function security when CT saturation is present. In [30], directional comparison units using phase, neutral, negative sequence and positive sequence currents are described. The last three units compensate the impact of load by using pure fault quantities. For ground faults, neutral current comparison features high dependability since the zero sequence network is highly homogeneous. The same applies for I2 comparison when the WT provides I2. Finally, pure fault comparison using I1-I1prefault is impacted by the pure fault positive sequence network non-homogeneity, as described in last section, but since the angular tolerance is high (120º is the default setting in [30]), it can be trusted.

5. TEST RESULTS

Previously mentioned protection functions were tested using Matlab Simulink® simulation of a Type III and IV WT. Faults on a 120kV were simulated using different line lengths, generated power, and fault resistance. In Table 2 the results for Type IV generation at 50% of the line and different faults and fault resistance are shown.

Table 2 Results for Type IV Generation

RF/RG (Ω)	Falta	67P	67ΔP	67Q	67P21	87P	87ΔP	87Q	φ_{I1}	φ_{I0}	φ_{V1}	φ_{V0}
0	AG	47º	121º	93º	87º	-45º	39º	10º	28º	-9º	180º	-3º
0	AB	48º	122º	84º	95º	-43º	39º	1º	92º	N/A	240º	N/A
0	ABG	48º	102º	80º	54º	-42º	20º	-2º	83º	127º	240º	120º
10	AG	52º	131º	86º	95º	-34º	48º	3º	37º	-3º	189º	2º
10	AB	53º	129º	85º	65º	-34º	46º	1º	97º	N/A	247º	N/A
10	ABG	75º	126º	87º	83º	-8º	43º	4º	72º	87º	240º	87º
50	BG	61º	160º	86º	67º	-5º	74º	-6º	170º	228º	-20º	238º
50	CG	62º	158º	86º	68º	-3º	74º	-8º	289º	108º	98º	118º
50	BCG	76º	142º	88º	98º	-1º	60º	-4º	190º	290º	0º	290º
50	CAG	75º	141º	88º	98º	-1º	59º	-5º	300º	170º	120º	168º

Angles that make the protection function work properly with typical settings are highlighted in green. The ones causing a malfunction are shown in red. In yellow are the ones that fall into the right angular zone but does not stabilize.

Since the Type IV model is adapted to comply with LVRT requirements, protection functions using I2 work properly, which would not happen in presence of legacy WTs not complying with the most actual grid codes.

In **¡Error! No se encuentra el origen de la referencia.** the results for Type III generation for a fault at 50% of the line are shown.

Table 3 Results for Type III Generation

RF/RG (Ω)	Falta	67P	67ΔP	67Q	67P21	87P	87ΔP	87Q	φ_{I1}	φ_{I0}	φ_{V1}	φ_{V0}
0	AG	75º	158º	88º	88º	-14º	74º	4º	59º	-4º	180º	-4º
0	AB	61º	166º	83º	84º	-28º	82º	0º	133º	N/A	240º	N/A
0	ABG	79º	132º	83º	82º	-9º	48º	0º	102º	119º	240º	115º
50	AG	53º	165º	92º	65º	-12º	82º	9º	64º	-8º	218º	-3º
50	BG	49º	162º	91º	64º	-15º	80º	7º	183º	234º	-23º	237º
50	CG	49º	162º	91º	64º	-15º	80º	7º	183º	234º	-23º	237º
50	ABG	110º	164º	86º	107º	21º	81º	3º	98º	49º	240º	49º
50	BCG	110º	164º	86º	107º	24º	83º	2º	220º	-40º	0º	288º
50	CAG	110º	164º	86º	107º	21º	81º	3º	338º	170º	120º	168º

In both cases, Type III and IV, phase selector angle φ_{I1} shows not to be trustable, since as it was seen before, pure fault positive sequence impedance is impacted by the control injection requirements. However, both voltage-based angles work correctly, despite of the fault resistance, whose impact stays within expected limits. Regarding the directional units, it is important to mention than zero sequence directional is another trustable element than can be used since the transformer supplies enough I0 to the fault.

For results shown in Table 3, an intermittent activation of the crowbar was observed, but it allowed the control to inject power accordingly to LVRT requirements. However, further simulations made, in which crowbar was forced to stay connected during the entire duration of the fault modified positive sequence angle since short circuiting the rotor makes the DFIG generator work as an induction machine, absorbing reactive power. This effect modifies ZL1S angle, as shown in Table 4, in which both fault and pure fault positive sequence directional units fail (67P, 67ΔP). With regard to pure fault positive sequence directional unit, it is very close to indicate an external fault as the default setting is 120º.

Table 4 Results for Type III with Crowbar active.

RF/RG (Ω)	Falta	67P	67ΔP	67Q	67P21	87P	87ΔP	87Q	φ_{I1}	φ_{I0}	φ_{V1}	φ_{V0}
0	AG	-50º	-165º	68º	80º	-125º	111º	-15º	116º	12º	178º	-8º
0	AB	-50º	-169º	69º	55º	-120º	105º	-14º	170º	N/A	240º	N/A
0	ABG	-50º	-180º	66º	49º	-136º	94º	-16º	167º	142º	240º	120º

It is possible to detect the long-lasting activation of the crowbar during the fault since it makes I2 injection be much higher than I1 (in the simulations done I2 was higher than 3 times I1). This is so because the impedance that the machine represents includes rotor and crowbar resistances, which for positive sequence is calculated as R/s but for negative sequence it is calculated as R/(2-s) [33]. As the slip is normally close to 0, $R/s \gg R/(2\text{-}s)$, which makes I2 much higher than I1. This condition could be used to block the units based on positive-sequence and enable the ones based on negative-sequence.

5.1.1   Apparent Fault Resistance Compensation

In Table 5 and 6, it is shown how the angular difference between the proposed polarization phasors and the current flowing through the fault resistance is close to zero. However, this does not happen with this last current and phase or phase to phase current (depending on fault type). Neither with pure fault phase or phase to phase currents. I0 polarization would remain a trustable polarization factor in this case.

Table 5 Polarization angle compensation, Type III

Crowbar Activation	Fault Type	RF (Ω)	Fpol Vs If angle difference (º)
Active	AG	50	-1,5
Active	AG	0	-1,2
Active	ABG	50	-1,1
Active	ABG	0	-1,3
Active	AB	50	-1,2
Active	AB	0	-1,3
Active	ABC	0	-1,2
No Active	AG	50	-1,5
No Active	AG	0	-0,6
No Active	ABG	50	-1,3

Table 6 Polarization angle compensation, Type IV

Fault Type	RF (Ω)	Fpol Vs If angle difference (º)
AG	50	-1,6
AG	0	-1,4
ABG	50	-1,3
ABG	0	-1,4
AB	50	-0,9
AB	0	-1,6
ABC	50	2,2
ABC	0	-0,6

No Active	ABG	0	-1,5
No Active	AB	50	-1,1
No Active	AB	0	-1,5
No Active	ABC	0	-1,2

6. CONCLUSIONS

Several conclusions might be extracted from the results observed. The impact of Type IV WTs on protection units using I2 depends fully on Grid Code compliance. Protection functions using I1 might be impacted depending on the value of k constant used by the control system for LVRT mode and the philosophy it uses to restrict different current components if the limit of the converter is reached. Type III fault response shows negative sequence impedance angle closer to the one shown by synchronous generation, but positive sequence impedance angle might be modified by the rotor protection methods.

Current based algorithms for phase selection are also impacted by the reaction speed of the control, which is not required to be faster than 60 ms per the Spanish grid code. Voltage based method is independent from the WT reaction speed and is therefore more trustable.

Apparent fault resistance compensation by calculating local source impedance was tested successfully for distance units.

As stated at the beginning of this work, most work started analyzing the impact of renewable energy on protection systems focused on the lack of I2 as the main threat, but once this issue has been minimized by grid codes, it is the angle of the injection of both sequence currents which might create the next challenges for protection engineers.

7. REFERENCES

[1] ENTSOE, "Short Circuit Contribution of New-Generating Units Connected with Power Electronics and Protection Behavior," April 3rd, 2019.

[2] R. A. Walling *et al*, "Current contributions from Type 3 and Type 4 wind turbine generators during faults," *Proceedings of the IEEE Power Engineering Society Transmission and Distribution,* 2012.

[3] Abdul W. Korai *et al*, "Generic DSL-Based Modeling and Control of Wind Turbine Type 4 for EMT Simulations in DIgSILENT PowerFactory," *Advanced Smart Grid Functionalities on PowerFactory,* 2018.

[4] V. Akhmatov *et al*, "Siemens Wind Power Variable-Speed Full Scale Frequency Converter Wind Turbine Model for Balanced and Unbalanced Short-Circuit Faults," *Wind Eng,* vol. 34, *(2)*, 2010.

[5] E. Farantatos *et al*, "Short-circuit current contribution of converter interfaced wind turbines and the impact on system protection," *2013 IREP Symposium Bulk Power System Dynamics and Control - IX Optimization, Security and Control of the Emerging Power Grid,* pp. 1-9, 2013.

[6] S. Seman *et al*, "Low voltage ride-through analysis of 2 MW DFIG wind turbine - grid code compliance validations," *2008 IEEE Power and Energy Society General Meeting - Conversion and Delivery of Electrical Energy in the 21st Century,* pp. 1-6, 2008.

[7] J. Lopez Taberna, "Comportamiento De Generadores Eólicos Con Máquina Asíncrona Doblemente Alimentada Frente a Huecos De Tensión." , Universidad Pública de Navarra, 2008.

[8] J. González and R. Lacal Arantegui, "Technological evolution of onshore wind turbines—a market-based analysis," *Wind Energy,* 2016.

[9] R. Teodorescu *et al*, *Grid Converters for Photovoltaic and Wind Power Systems.* John Wiley & Sons, 2011.

[10] Microsemi Corporation, "Park, Inverse Park and Clarke, Inverse Clarke Transformations MSS Software Implementation," 2013.

[11] N. Tleis, "6 - Modelling of voltage-source inverters, wind turbine and solar photovoltaic (PV) generators," *Power Systems Modelling and Fault Analysis (Second Edition),* pp. 469-596, 2019.

[12] I. Erlich *et al*, *Wind Turbine Negative Sequence Current Control and its Effect on Power System Protection.* 2013.

[13] A. D. Hansen *et al*. Dynamic wind turbine models in power system simulation tool DIgSILENT. Danmarks Tekniske Universitet, Risø Nationallaboratoriet for Bæredygtig Energi.

[14] F. K. A. Lima *et al*, "Rotor Voltage Dynamics in the Doubly Fed Induction Generator During Grid Faults," *IEEE Transactions on Power Electronics,* vol. 25, *(1),* pp. 118-130, 2010.

[15] J. Rodríguez Arribas *et al*, "Low Voltage Ride-through in DFIG Wind Generators by Controlling the Rotor Current without Crowbars," *Energies,* vol. 7, *(2),* pp. 498-519, 2014.

[16] A. D. Hansen and G. Michalke, "Fault ride-through capability of DFIG wind turbines," *Renewable Energy,* vol. 32, *(9),* pp. 1594-1610, 2007

[17] Y. Zhou *et al*, "Operation of Grid-Connected DFIG Under Unbalanced Grid Voltage Condition," *IEEE Transactions on Energy Conversion,* vol. 24, *(1),* pp. 240-246, 2009. . DOI: 10.1109/TEC.2008.2011833.

[18] O. P. Mahela *et al*, "Comprehensive Overview of Low Voltage Ride Through Methods of Grid Integrated Wind Generator," *IEEE Access,* vol. 7, pp. 2019.

[19] L. Peng, B. Francois and Y. Li, "Improved crowbar control strategy of DFIG based wind turbines for grid fault ride-through," in *2009 Twenty-Fourth Annual IEEE Applied Power Electronics Conference and Exposition,* 2009, .

[20] Maoze Wang *et al*, "A new control system to strengthen the LVRT capacity of DFIG based on both crowbar and DC chopper circuits," in *IEEE PES Innovative Smart Grid Technologies,* 2012.

[21] G. N. Sava *et al*, "Comparison of active crowbar protection schemes for DFIGs wind turbines," in *2014 16th International Conference on Harmonics and Quality of Power (ICHQP),* 2014, .

[22] G. Pannell *et al*, "Evaluation of the Performance of a DC-Link Brake Chopper as a DFIG Low-Voltage Fault-Ride-Through Device," *IEEE Transactions on Energy Conversion,* vol. 28, *(3),* pp. 535-542, 2013. .

[23] M. M. Shabestary and Y. A. I. Mohamed, "Asymmetrical Ride-Through and Grid Support in Converter-Interfaced DG Units Under Unbalanced Conditions," *IEEE Transactions on Industrial Electronics*, 2019.

[24] S. Alepuz *et al*, "Control Strategies Based on Symmetrical Components for Grid-Connected Converters Under Voltage Dips," *IEEE Trans. Ind. Electron.,* vol. 56, *(6),* pp. 2162-2173, 2009.

[25] Ö. Göksu *et al*, "Impact of wind power plant reactive current injection during asymmetrical grid faults," *IET Renewable Power Generation,* vol. 7, *(5),* 2013.

[26] T. Neumann and I. Erlich, "Modelling and control of photovoltaic inverter systems with respect to German grid code requirements," *2012 IEEE Power and Energy Society General Meeting,* pp. 1-8, 2012.

[27] A. Camacho *et al*, "Positive and Negative Sequence Control Strategies to Maximize the Voltage Support in Resistive-Inductive Grids During Grid Faults," *IEEE Transactions on Power Electronics,* 2018.

[28] A. Haddadi *et al*, "Negative sequence quantities-based protection under inverter-based resources Challenges and impact of the German grid code," *Electr. Power Syst. Res*

[29] ZIV APLICACIONES Y TECNOLOGÍA, "Manual de Instrucciones para Modelos DLF", 2019.

[30] R.Cimadevilla. Improvements in the operation of a distance relay during resistive faults. TEXAS A&M 2014

[31] ZIV APLICACIONES Y TECNOLOGÍA, "Manual de Instrucciones para Modelos ZLF", 2019.

[32] R.Cimadevilla. New protection units included in differential relays. PAC Conference 2011

[33] S. E. Zocholl. Induction Motors: Part I – Analysis. *Schweitzer Engineering Laboratories, Inc.* 2017

8. BIOGRAPHICAL DATA

Roberto Cimadevilla graduated in Electrical Engineering from the Superior Engineering College of Gijón, Spain in 2001. He did his final year project at the University of Dundee, Scotland, and obtained a master´s degree in "Analysis, simulation and management of electrical power systems" at the University of País Vasco, Spain. He started his professional career in the protection maintenance area of Red Eléctrica de España (Spanish TSO). Roberto joined ZIV in 2003, where he actively participated in the development of several protection and control devices, including distance, transformer differential, line differential and feeder relays. Roberto has held several positions of technical and management responsibility inside ZIV. He is currently the Manager of the Application Engineering Department of the Substation and Distribution Automation (ZIV DASA) Product Line. Roberto has written more than 25 papers, he is an IEEE member and has participated in several CIGRE working groups.

Alberto Castañón was born in Tixtla, México en 1990. Graduated and Electromechanical Engineer by the Monterrey Institute of Superior Technological Studies in 2014. Between 2014 and 2019 worked as an Electrical Engineer for General Electric in the Gas Turbine. In 2009 he studies a Masters about Renewable Energy Integration on the Electrical Grid by the University of País Vasco, Spain, writing its final thesis by ZIV, which he joined as an application engineer up to now.

Pablo Eguia, born in Bilbao in 1973, graduated as Industrial Engineer (1998) by the UPV/EHU and PhD in Industrial Engineering (2007) by the same university. He is principal researcher for the GISEL

group. Pablo has participated in 36 research projects in competitive public calls and more than 78 with private companies. During the last years of his work, he has been focused on modeling electrical systems for the integration of distributed generation, actively collaborating with several companies of the industry in the Basque Country. He is director for three PhD thesis, coauthor of 25 articles in index publications, more than 90 lectures in international congresses, 7 book chapters and 2 international CIGRE reports. He is a member of the IEEE and CIGRE, has participated in several international work groups ion the field of protection and control of electrical systems and is an evaluator of different international magazines (IEEE PWRD, IEEE PWRS, Energy, etc.). He has two research six-year terms and one transference one. He has been awarded with the Euskoiker research price in 2010 in the Engineering and Technology area.

Esther Torres was born in Bilbao in 1972. She received her Industrial Engineering degree by the UPV/EHU in 1998 and PhD in Industrial Engineering (2008) by the same university. Since 1999 works as professor on the Electrical Engineering Department of the Bilbao School of Engineering. She is codirector of three PhD thesis and has collaborated in 23 I+D competitive research projects and 28 research contracts with private companies. During the last year her research activity has focused on the modeling of electrical systems for the integration of distributed generation. She is coauthor of 16 articles in scientific publications and 81 congress lectures, 4 book chapters and two CIGRE technical reports. She has two research six-year periods.

Ricardo Ibarra, born in Vitoria in 1997, graduated as Renewable Energy Engineer in 2020 by the UPV/EHU. He is currently finalizing its master studies "Renewable Energy Integration in the Electrical System" in the same university, and it is doing its Master Thesis in collaboration with ZIV about fault detection in electrical grid with high penetration of generation based on renewable energy.